JTE HCMUTE
ISSN: 2615-9740

JOURNAL OF TECHNICAL EDUCATION SCIENCE
Ho Chi Minh City University of Technology and Education
Website: https://jte.hcmute.edu.vn/
Email: jte@hcmute.edu.vn

Global Analysis of Three-Dimensional Shape Symmetry: Human Skulls (Part II)

Vi-Do Tran[1], Tien-Tuan Dao[2], Tan-Nhu Nguyen[2*]

[1] *HCM City University of Technology and Education, Ho Chi Minh City, Vietnam*
[2] *Univ. Lille, CNRS, Centrale Lille, UMR 9013 – LaMcube – Laboratoire de Mécanique, Multiphysique, Multiéchelle, 59655 Villeneuve d'Ascq Cedex, F-59000, Lille, France*

[*] Corresponding author. *Email: nhunguyentan@gmail.com*

ARTICLE INFO

Received: 23/2/2022
Revised: 14/8/2022
Accepted: 24/8/2022
Published: 30/8/2022

KEYWORDS

Facial paralysis grading;
Muscle action lengths;
Global geometrical symmetry;
Skull global symmetry;
Facial mimic rehabilitation.

ABSTRACT

Facial mimics are important to human life, so facial palsy negatively affects the involved patients. Recently, the comparison of muscle action lengths between the left and right-hand sides has been used to evaluate facial palsy quantitatively. However, even in the healthy subjects, their left and right muscle action lengths could not be perfectly symmetrical. These action lengths were formed by insertion points on the head and attachment points on the skull. Consequently, the geometrical dissymmetry between left and right human skulls needs to be analyzed and reported quantitatively. So far, no studies have reported this quantity. In this paper, in the second part of our study, we analyzed symmetrical levels between the left and right sides of human skulls. In particular, 329 skull models reconstructed from computed tomography (CT) images of healthy subjects in neutral mimics were used for calculating. The left and right skull regions were mirrored through a center plane of the skull. Hausdorff distance and volumetric differences between the left skulls (skull convex hulls) and mirrored right skulls (skull convex hulls) were computed as the distance and volumetric symmetries, respectively. As a result, the distance dissymmetrical values (Mean ± SD) are 1.2680 ± 0.3538 mm, and ones of volumetric dissymmetry (Mean ± SD) are 32.1790 ± 23.2725 cm^3. In perspective, we will analyze the skull symmetry in more detail with different local shape topologies. Moreover, the global and local shape symmetries will be implemented in our clinical decision support system for facial mimic rehabilitation.

DOI: https://doi.org/10.54644/jte.71A.2022.1143

1. Introduction

Facial mimics are important to both the personal and professional lives of humans [1], so facial palsy negatively affects the involved patients [2]. Facial paralysis grading is the first required step for evaluating the levels of facial palsy before conducting rehabilitation treatments [3]. Facial paralysis grading methods include clinical [4] and non-clinical [4] approaches. Because of the quantitative and objective characteristics, non-clinical methods have been popularly employed [4]. After grading, clinicians have to diagnose the level of facial palsy based on their clinical expertise [3].

Currently, we have developed a novel non-clinical facial paralysis-grading concept, which is based on an analysis of muscle action lengths on the left and right heads [5]. The muscle action lines were constructed from muscle insertion points on the skin layer of the head and muscle attachment points on the bone layer of the skull [6]–[13]. Especially, even in healthy subjects, muscle action lengths on the left and right-hand sides were not perfectly symmetrical [5]. If these muscle action lengths were directly applied without considering the symmetries of the head and skull of healthy subjects, the system [14] will misclassify the patients among the healthy subjects. Based on our hypothesis, the symmetries of head and skull shapes affect the symmetries of the muscle action lines. Moreover, because we used the Euclidian distance metric for evaluating the muscle action lines between the left and right-hand sides [5], the distance metric should be used for computing the head and skull shape's symmetries. Additionally, to clearly describe the 3-D geometrical differences, the volume metric should also be employed. The computed values could be used as thresholds for classifying and analyzing the patients

among the healthy subjects. In the first part of our study, we reported these symmetrical values of the head [15]. In this second part, we will analyze more about the dissymmetry of the human skull. No studies in the literature have analyzed this dissymmetry on the human skull.

It is important to note that, recently, most non-clinical facial paralysis grading used 2-D geometrical information in color images for analyzing facial paralysis levels. These metrics could be pixel value differences, 2-D coordinates of facial features, etc [16]. These studies preferred to use color images because these features could be easily detected in real-time [17], [18]. However, the pixel values in images were very sensitive to light conditions and lacked the third dimension. Consequently, 3-D geometrical information could be a better choice [19]–[22]. Additionally, in our previous study, we can animate subject-specific head models in real-time [23]. This could help evaluate facial paralysis more robustly when using 3-D geometrical metrics. The most popular 3-D metrics are distances and volumes [21], [22]. Some studies also tried to study symmetries of human skulls, but they just analyzed 2-D geometrical information in original CT images not in 3-D models [24]. Consequently, in this study, analyzing symmetries of skulls based on 3-D distances and volumes is suitable and novel for enhancing the accuracy of real-time facial paralysis grading.

In particular, the dataset of 329 skull models has been reconstructed from the computed tomography (CT) images of healthy subjects in neutral mimics. All skull models were cut into left and right regions from the middle of the skulls. The left and right skulls were then mirrored through the middle plane. Mean Hausdorff distance differences between the left skulls and mirrored right skulls were computed as the distance symmetry quantity. Moreover, volumetric differences between the left skull convex hulls and the mirrored skull convex hulls were also computed as the volumetric symmetry quantity. As a result, the distance dissymmetrical values (Mean ± SD) are 1.2680 ± 0.3538 mm, and the volumetric dissymmetrical values (Mean ± SD) are 32.1790 ± 23.2725 cm^3.

The reported values partially help explain how muscle action lengths were not perfectly symmetrical even in the healthy subjects. These values could also be implemented in the muscle-based facial paralysis grading for automatically diagnosing facial palsy. In perspective, the skull symmetry will be analyzed in more detail with various local topological shapes. Moreover, these values will be implemented in our clinical decision support system for facial mimic rehabilitation [25].

2. Methods

2.1. Datasets

The dataset included 329 skull models (male: 265, female: 64, ages (Mean ± SD): 61 ± 11 years) reconstructed from CT images of facial healthy subjects in neutral mimics. The CT image dataset was downloaded from the public The Cancer Imaging Archive (TCIA) [26]. The CT images (DICOM 512×512) were selected so that they have full skull structure in all captured slices. The reconstruction process was conducted using the 3DSclicer open-source tool. Details of the reconstruction procedure were presented in our previous study [27]. After being reconstructed, the skulls were post-processed so that they just contain the skull structure and have approximately the same number of vertices. The reconstruction and post-processing procedures were clearly explained in our previous study [27]. Moreover, because of the limitation of CT image quality, some small structures of the skulls could not be reconstructed. Consequently, the skull shapes were also generated from the skull models for capturing only the global shape information. The detailed process of skull shape generation was presented in our previous study [27]. For supporting the dataset normalizing procedure, feature points were also manually selected on each skull model. The illustration of a skull model with feature points and a skull shape in the dataset was in Figure 1.

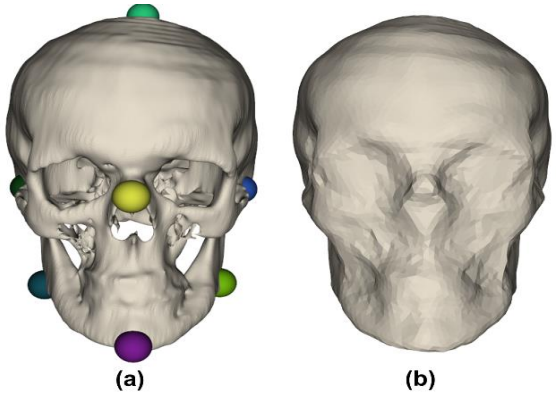

Figure 1. *Skull model with feature points and skull shape: (a) skull model with feature points and (b) skull shape generated from the skull model.*

2.2. Overall Processing Procedure

The overall processing procedure is shown in Figure 2. In particular, all skull models were first registered to the same coordinate system with a template skull during *Skull Orientation Fixing*. In *Left/Right Skull Cutting*, all registered skulls were cut into left and right regions based on a bounding box cutting technique. The left and right skulls were then mirrored through the center plane using a reflecting transform in the *Left/Right Skull Mirroring*. Finally, Hausdorff distances between the left skulls and the mirrored right skulls were computed as the distance symmetrical level in *Hausdorff Distance Computing*. Moreover, volumetric differences between the left skull convex hulls and the mirrored right convex hulls were also computed for volumetric symmetrical levels in *Volumetric Computing*. Moreover, distance errors and volumetric differences were also computed between the right skulls (skull convex hulls) and the mirrored left skulls (skull convex hulls).

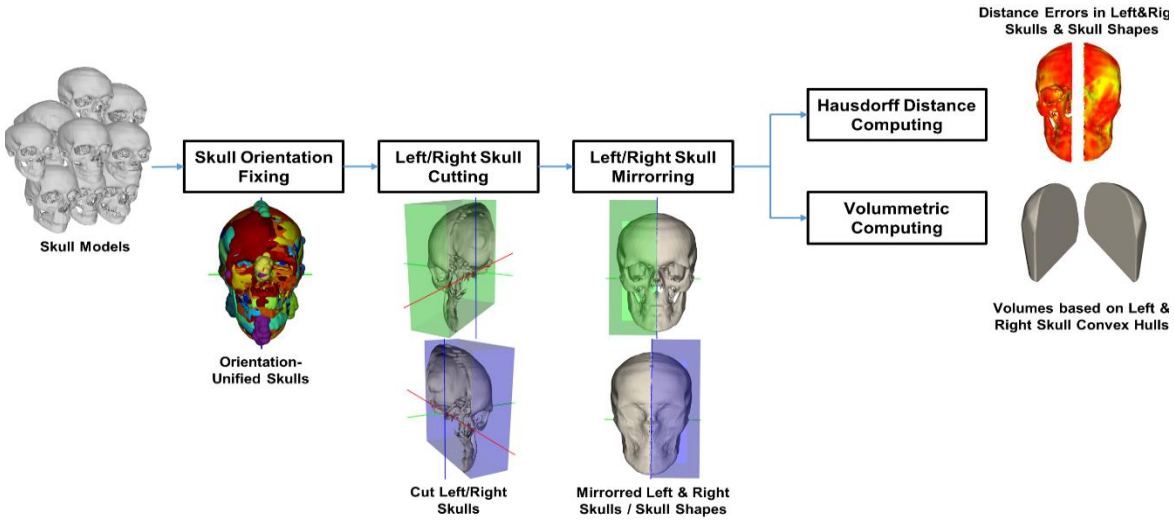

Figure 2. *The overall processing procedure of the global skull symmetry analysis.*

2.3. CT-based Skull Normalization

All skull models need to be optimally in the vertical direction with the global space. To do that, all skulls were optimally registered to the same coordinate system with the template skull, which was perfectly in the vertical direction in the global space. The template skull (Figure 3a) was used in our previous study for deforming the other skull [27]. This template skull was manually designed in computer-aided design (CAD) software, so it has perfect geometrical symmetry [27]. In this template skull, we also selected feature points, as shown in Figure 3a. The template skull was registered to the global space so that the Feature Point (FP) 0 was on the x-axis, FP2 & FP4 were on the y-axis, and FP6 was on the z-axis. This strategy guaranteed that the template skull was exactly in the vertical direction (Figure 3b).

JTE
HCMUTE
ISSN: 2615-9740

JOURNAL OF TECHNICAL EDUCATION SCIENCE
Ho Chi Minh City University of Technology and Education
Website: https://jte.hcmute.edu.vn/
Email: jte@hcmute.edu.vn

Each skull model in our dataset was registered to the same coordinate system as the template skull using the singular value decomposition (SVD) rigid registration method [28] based on the feature points on the skull (Figure 1a) and the feature points on the template skull (Figure 3a). To eliminate the errors from the manual feature point selection, the coherent point drift (CPD) rigid registration method [29] was then used to optimally register the skull vertices to the template skull vertices. It is important to note that the CPD registration method estimates the probabilistically optimal rigid transform between two point sets. Consequently, after using the CPD the skull model was optimally on the same coordinate system as the template skull model (Figure 3c).

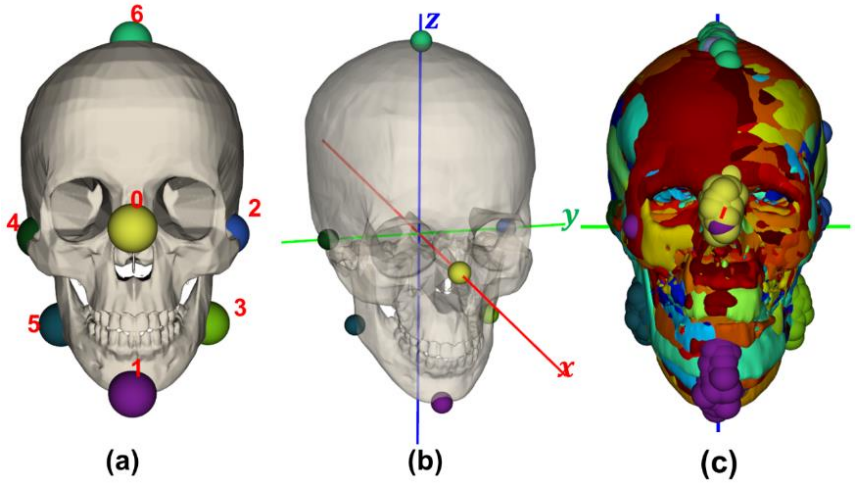

Figure 3. *Skull orientation fixing: (a) template skull with feature points, (b) orientation-fixed template skull on the global space, and (c) registered skulls on the same coordinate system with the template skull.*

2.4. Estimation of ROI Boxes and Left & Right Skull Cutting

The left and right bounding boxes were estimated for each registered skull in our dataset. A full bounding box was defined so that its four corners must form a box covering exactly all vertices of the skull (Figure 4a). The left bounding box was defined as the half-left part of the full bounding box (Figure 4b, c), and the right bounding box was defined as the half-right part of the full bounding box (Figure 4b, d). The left skull region has the vertices and facets of the skull inside the left bounding box. The right skull region has the vertices and facets of the skull inside the right bounding box. Moreover, the left skull shape has the vertices and facets of the skull shape inside the left bounding box, and the right skull shape has the vertices and facets of the skull shape inside the right bounding box.

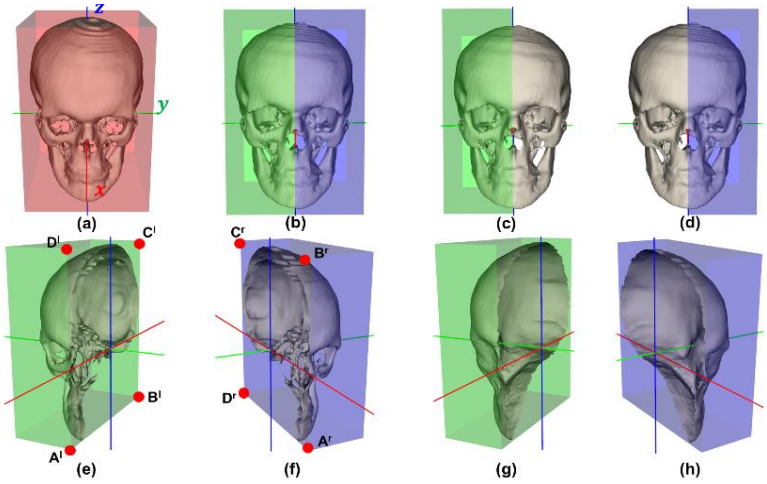

Figure 4. *Left and right bounding boxes generated from a full bounding box and left & right head cutting using the left & right bounding boxes: (a) full bounding box, (b) left & right bounding boxes, (c) left bounding box, (d) right bounding box, (e) left skull region, (f) right skull region, (g) left skull shape region, and (h) right skull shape region.*

JTE
HCMUTE
ISSN: 2615-9740

JOURNAL OF TECHNICAL EDUCATION SCIENCE
Ho Chi Minh City University of Technology and Education
Website: https://jte.hcmute.edu.vn/
Email: jte@hcmute.edu.vn

2.5. Left & Right Skull Mirroring

For mirroring the left and right skulls (skull shapes), we used the reflecting Householder transform [30]. In this transform, all vertices of a left (right) skull (skull shape) were mirrored through a reflecting plane. The reflecting plane was formed from (A^l B^l C^l D^l) or (A^r B^r C^r D^r). In which, A^l, B^l, C^l, D^l, A^r, B^r, C^r, and D^r are the four corners of the left (l) bounding boxes (Figure 4e) and the right (r) bounding box (Figure 4f). The facets of the mirrored left (right) skull (skull shape) are the facets of the left (right) skull (skull shape) with inversed directions. Figure 5 shows the mirrored left (right) skull (skull shape) from the left (right) skull (skull shape). As a result, the left & right skulls and the mirrored left & right skulls were ready for symmetrical analyses.

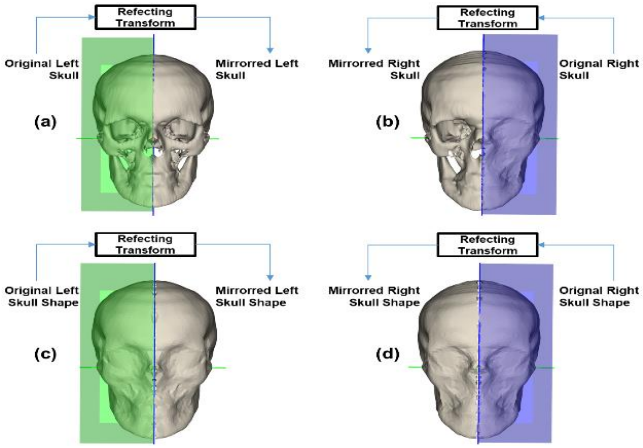

Figure 5. *Left & right skull and skull shape mirroring using reflecting from through the central plane of the bounding box.*

2.6. Distance Symmetry Analysis

For analyzing the distance symmetry of all skulls in the dataset, all left skulls (skull shapes) were compared with all mirrored right skulls (skull shapes). Moreover, all right skulls (skull shapes) were also compared with all mirrored left skulls (skull shapes). The Hausdorff distance metric [31] was used for these comparisons. In the Hausdorff, surface differences between the first and second models were represented as Euclidean distances between the vertices on the first model and their nearest vertices on the second model. For each subject, the mean Hausdorff distance was computed between the left (right) skull (skull shape) and the mirrored right (left) skull (skull shape), respectively. Figure 6 shows examples of computed Hausdorff distances represented as color maps on the left (right) skull (skull shape).

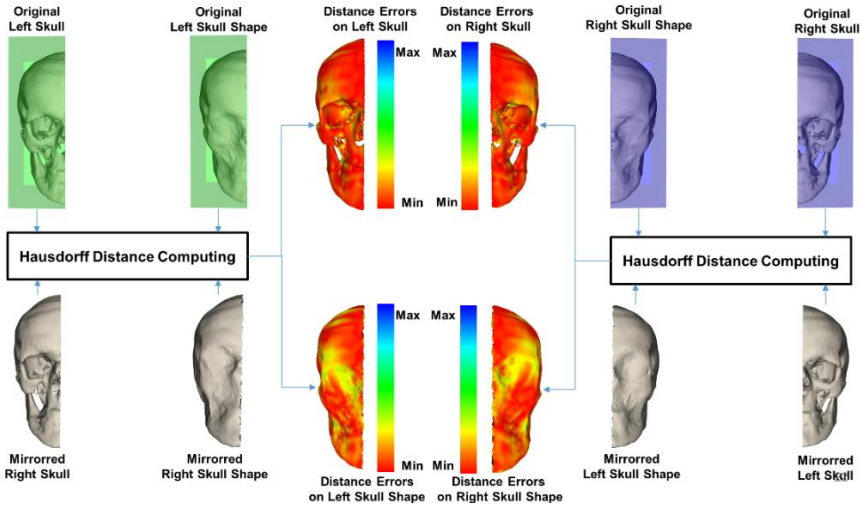

Figure 6. *Distance symmetrical analysis between the left (right) skull (skull shape) and the mirrored right (left) skull (skull shape), respectively.*

JTE
HCMUTE
ISSN: 2615-9740

JOURNAL OF TECHNICAL EDUCATION SCIENCE
Ho Chi Minh City University of Technology and Education
Website: https://jte.hcmute.edu.vn/
Email: jte@hcmute.edu.vn

2.7. Volumetric Symmetry Analysis

Because the left (right) skull models and the mirrored right (left) skull models were not closed surfaces, so we could not estimate directly their internal volumes. Consequently, the convex hulls of the left (right) skulls and the mirrored right (left) skull convex hulls were used instead (Figure 7). For all subjects, volumetric differences between the left (right) skulls and the mirrored (right) left skulls were computed as the volumetric symmetrical values. The volumes were computed using the available function in the CGAL mesh-processing library CGAL::Polygon_mesh_processing::volume [32].

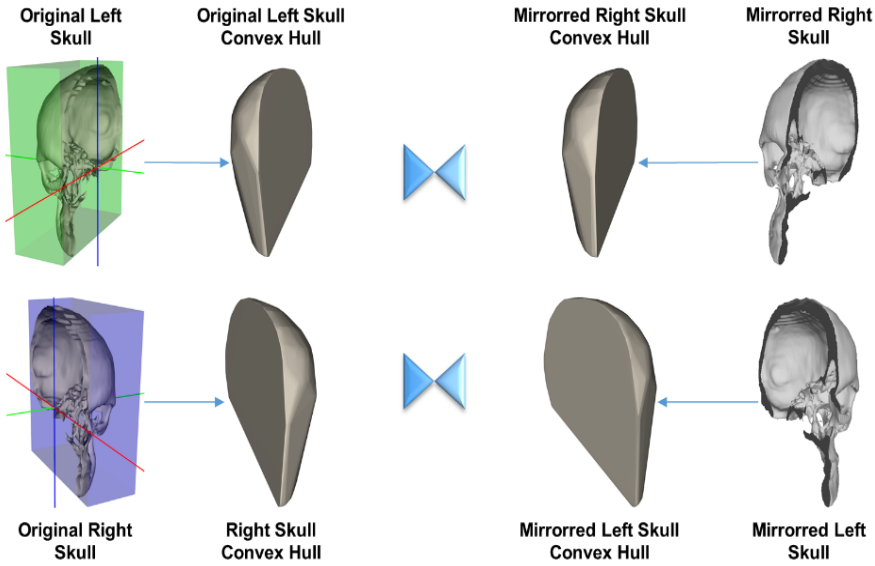

Figure 7. *Volumetric symmetrical analysis between the left (right) skull convex hulls and the mirrored right (left) convex hulls, respectively.*

3. Results and Discussion

Mean Hausdorff distances between the left (right) skulls (skull shapes) and the mirrored right (left) skull (skull shapes), respectively, are shown in Figure 8. Between the left skulls and the mirrored right skulls, the distance dissymmetrical values (Mean ± SD) are 1.3403 ± 0.2601 mm. The distance symmetrical values between the right skulls and the mirrored left skulls are 1.3664 ± 0.2791 mm. Distance symmetrical values (Mean ± SD) between the left skull shapes and mirrored right skull shapes are 1.2680 ± 0.3538 mm, and ones between the right skull shapes and mirrored left skull shapes are 1.2855 ± 0.3665 mm. Based on the result, we can see that dissymmetrical values of the skulls are larger than ones of the skull shapes. This is because of the limitation of the CT scanning quality, so some small internal structures could be successfully reconstructed on the left skull regions, but not on the right skull regions (and vice versa). If we just focused on the global shape of the skull, skull shape dissymmetrical values are suitable for this purpose. Additionally, the dissymmetrical values between the left skulls (skull shapes) and the mirrored right skulls (skull shapes) are relatively the same as the ones between the right skulls (skull shapes) and the mirrored left skulls (skull shapes). Consequently, we can only use the symmetrical values between the left skulls (skull shapes) and mirrored right skulls (skull shapes) for representing the distance symmetry of the human skull. Moreover, if only the overall shape of the skull is needed, the skull shape's symmetrical values are enough.

Volumetric differences between the left (right) skull convex hulls and the mirrored right (left) skull convex hulls are reported in Figure 9. The volumetric symmetrical values between the left skull convex hulls and the mirrored right skull convex hulls are the same as the ones between the right skull convex hulls and the mirrored left skull convex hulls. These values (Mean ± SD) are 32.1790 ± 23.2725 cm^3.

In this study, we tried to analyze geometrical symmetries between the left and right skulls for 329 skull models of healthy subjects in neutral facial mimics. Compared with the first part of our study, which analyzed symmetries of human heads for healthy subjects, in this part, we targeted the human skulls. Regarding the methods, we applied the same data normalization techniques as in the previous

JTE
HCMUTE
ISSN: 2615-9740

JOURNAL OF TECHNICAL EDUCATION SCIENCE
Ho Chi Minh City University of Technology and Education
Website: https://jte.hcmute.edu.vn/
Email: jte@hcmute.edu.vn

part. However, because the skull structure contains complex anatomy inside, in this study, we tried to estimate the convex hulls of the skulls. Finally, the distance and volumetric symmetries were computed on the estimated skulls' convex hulls. It is important to note that because muscle attachment points are only on the external structures of the skulls, we can use the convex hulls of the skulls stead of the original skulls for analyzing the symmetries. Additionally, using convex hulls, we can easily estimate the 3-D volumes.

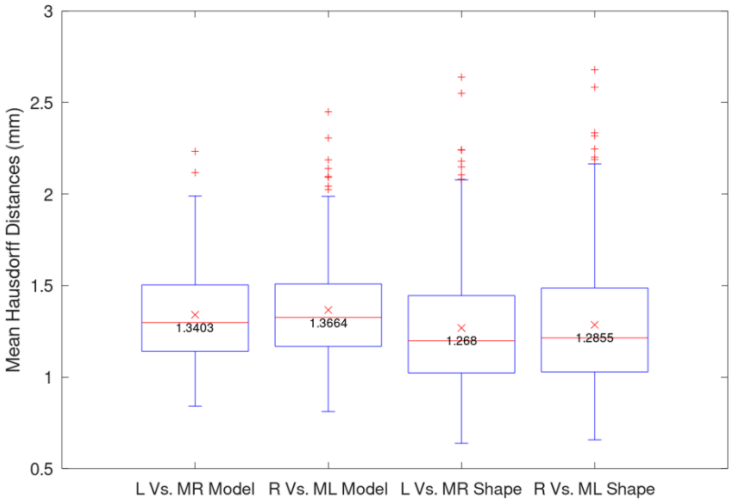

Figure 8. *Mean Hausdorff distances between the left (right) skulls (skull shapes) and the mirrored right (left) skulls (skull shapes).*

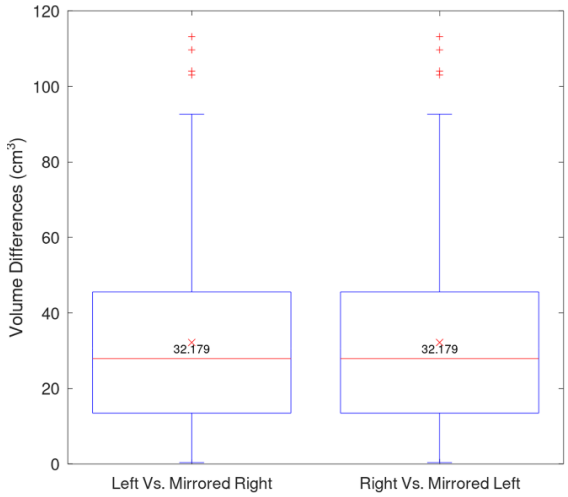

Figure 9. *Volumetric differences between the left (right) skull convex hulls and the mirrored right (left) skull convex hulls.*

The symmetrical values of human heads contributed to the dissymmetry between the left and right muscle action lengths [5]. Based on the reported values in this second part of our study, we can conclude that even the healthy subjects, their skulls are not perfectly symmetrical. This conclusion also partially helped explain why muscle action lengths between the left and right muscles were not perfectly symmetrical [5]. Moreover, because the muscle action lines were formed from the insertion points on the skin layer to the attachment points on the skull layer, dissymmetrical values on the skulls could be used to infer the dissymmetrical values of the muscle lines when being combined with the dissymmetrical values of the heads. Some studies also tried to compute symmetries of human skulls [33], but they only computed on 2-D geometrical metrics in original CT images [33]. In this study, we first reported the symmetrical values including distance and volume metrics in 3-D skull models reconstructed from CT images. These values are important to anatomy analysis and diagnosis [24].

Dissymmetrical values of the muscle lines could be applied to diagnose facial palsy in the non-clinical muscle-based facial paralysis grading methods automatically. In particular, in our current clinical decision-support system for facial mimic rehabilitation, subject-specific head models could be fast generated. The biomechanical head models which include the head, skull, and muscle network, could be animated in real-time with acceptable accuracy [5]. Moreover, we could also compute head muscle network symmetries in real-time. However, we lacked the functions of facial paralysis diagnoses that can detect and grade the level of facial paralysis. The values of distance and volume differences between the left and right-hand-side of the heads and skulls will be used as thresholds for detecting abnormal muscle behaviors. The abnormal levels will be computed as how far the current symmetry values are from the thresholds.

In perspective, we will analyze both human heads and skulls in more detail with different local topological shapes (e.g. eyes, nose, mouth, jaws, etc.). In further studies, we will compute skull symmetries locally in the muscle attachment points on the skull shapes. The muscle attachment points will be automatically detected by using a template skull with pre-defined muscle attachment points. Regions of interest (ROIs) defined by the muscle attachment points and a given radius were used for narrowing the local regions of the skull. Skull parts covered by the ROIs will be compared with their mirrored parts for evaluating the symmetries. All local and global symmetrical values will be implemented in our clinical decision support system for facial mimic rehabilitation to automatically diagnose facial palsy.

4. Conclusions

In this second part of our study, we have tried to report the global geometrical symmetry values of human skulls. As a result, the distance dissymmetrical values (Mean ± SD) are 1.2680 ± 0.3538 mm, and volumetric dissymmetrical values (Mean ± SD are 32.1790 ± 23.2725 cm^3. Because skull structures affect the strains of facial muscle during their motions, these values are important to facial paralysis grading applications based on muscle strains. In particular, these values are important thresholds for classifying symmetries of healthy subjects and patients [5]. In perspective, both human heads and skulls will be analyzed in more detail with various local topological shapes. Both local and global topological shape symmetrical values will also be implemented in our clinical decision support system for facial mimic rehabilitation [25]. In particular, the symmetrical values of both head and skull both globally and locally will be used as thresholds of left and right muscle length differences. These thresholds will be used for enhancing automatically facial paralysis classification and diagnosing.

Acknowledgments

This work belongs to the project grant No: B2022-SPK-01 funded by the Ministry of Education and Training, and hosted by Ho Chi Minh City University of Technology and Education, Vietnam.

REFERENCES

[1] C. Frith, “Role of facial expressions in social interactions,” *Philos. Trans. R. Soc. B Biol. Sci.*, vol. 364, no. 1535, pp. 3453–3458, Dec. 2009.
[2] L. E. Ishii, J. C. Nellis, K. D. Boahene, P. Byrne, and M. Ishii, “The Importance and Psychology of Facial Expression,” *Otolaryngol. Clin. North Am.*, vol. 51, no. 6, pp. 1011–1017, 2018.
[3] M. W. Robinson and J. Baiungo, “Facial Rehabilitation: Evaluation and Treatment Strategies for the Patient with Facial Palsy,” *Otolaryngol. Clin. North Am.*, vol. 51, no. 6, pp. 1151–1167, 2018.
[4] W. S. W. Samsudin and K. Sundaraj, “Clinical and non-clinical initial assessment of facial nerve paralysis: A qualitative review,” *Biocybern. Biomed. Eng.*, vol. 34, no. 2, pp. 71–78, 2014.
[5] T.-N. Nguyen, S. Dakpe, M.-C. Ho Ba Tho, and T.-T. Dao, “Kinect-driven Patient-specific Head, Skull, and Muscle Network Modelling for Facial Palsy Patients,” *Comput. Methods Programs Biomed.*, p. 105846, Nov. 2020.
[6] T. Wu, A. P. L. Hung, P. Hunter, and K. Mithraratne, “Modelling facial expressions: A framework for simulating nonlinear soft tissue deformations using embedded 3D muscles,” *Finite Elem. Anal. Des.*, vol. 76, pp. 63–70, 2013.
[7] A. X. Fan, S. Dakpé, T. T. Dao, P. Pouletaut, M. Rachik, and M. C. Ho Ba Tho, “MRI-based finite element modeling of facial mimics: a case study on the paired zygomaticus major muscles,” *Comput. Methods Biomech. Biomed. Engin.*, vol. 20, no. 9, pp. 919–928, 2017.
[8] T. T. Dao, A. X. Fan, S. Dakpé, P. Pouletaut, M. Rachik, and M. C. Ho Ba Tho, “Image-based skeletal muscle coordination: case study on a subject specific facial mimic simulation,” *J. Mech. Med. Biol.*, vol. 18, no. 2, pp. 1–15, 2018.
[9] Y. Lee, D. Terzopoulos, and K. Waters, “Constructing physics-based facial models of individuals,” *Proc. Graphics Interface’93 Conf.* , 1993, pp. 1–8.
[10] K. Kähler, J. Haber, and H.-P. Seidel, “Geometry-based muscle modeling for facial animation,” in *Graphics interface*, 2001, vol. 2001, pp. 37–46.
[11] P. Claes, D. Vandermeulen, S. De Greef, G. Willems, J. G. Clement, and P. Suetens, “Computerized craniofacial reconstruction:

Conceptual framework and review," *Forensic Sci. Int.*, vol. 201, no. 1–3, pp. 138–145, 2010.
[12] M. Wei, Y. Liu, H. Dong, and A. El Saddik, "Human Head Stiffness Rendering," *IEEE Trans. Instrum. Meas.*, vol. 66, no. 8, pp. 2083–2096, 2017.
[13] H. Y. Ping, L. N. Abdullah, P. S. Sulaiman, and A. A. Halin, "Computer Facial Animation: A Review," *Int. J. Comput. Theory Eng.*, vol. 5, no. 4, pp. 658–662, 2013.
[14] T.-N. Nguyen, "Clinical decision support system for facial mimic rehabilitation," *Compiègne*, 2020.
[15] V.-D. Tran, T.-T. Dao, T.-N. Nguyen, and others, "Global Analysis of Three-Dimensional Shape Symmetry: Human Heads (Part I)," *J. Tech. Educ. Sci.*, no. 68, pp. 27–35, 2022.
[16] S. Wang, H. Li, F. Qi, and Y. Zhao, "Objective facial paralysis grading based onP face and eigenflow," *Med. Biol. Eng. Comput.*, vol. 42, no. 5, pp. 598–603, Sep. 2004.
[17] M. Frey *et al.*, "3D Video Analysis of Facial Movements," *Facial Plast. Surg. Clin. North Am.*, vol. 19, no. 4, pp. 639–646, 2011.
[18] M. D. Salgado, S. Curtiss, and T. T. Tollefson, "Evaluating symmetry and facial motion using 3D videography," *Facial Plast. Surg. Clin. North Am.*, vol. 18, no. 2, pp. 351–356, 2010.
[19] H. Popat, E. Henley, S. Richmond, L. Benedikt, D. Marshall, and P. L. Rosin, "A comparison of the reproducibility of verbal and nonverbal facial gestures using three-dimensional motion analysis," *Otolaryngol. - Head Neck Surg.*, vol. 142, no. 6, pp. 867–872, 2010.
[20] P. A. Desrosiers, Y. Bennis, M. Daoudi, B. Ben Amor, and P. Guerreschi, "Analyzing of facial paralysis by shape analysis of 3D face sequences," *Image Vis. Comput.*, vol. 67, pp. 67–88, 2017.
[21] D. Gibelli, D. De Angelis, P. Poppa, C. Sforza, and C. Cattaneo, "An Assessment of How Facial Mimicry Can Change Facial Morphology: Implications for Identification," *J. Forensic Sci.*, vol. 62, no. 2, pp. 405–410, 2017.
[22] C. Tanikawa and K. Takada, "Test-retest reliability of smile tasks using three-dimensional facial topography," *Angle Orthod.*, vol. 88, no. 3, pp. 319–328, 2018.
[23] T. N. Nguyen, S. Dakpe, M. C. Ho Ba Tho, and T. T. Dao, "Real-time Subject-specific Head and Facial Mimic Animation System using a Contactless Kinect Sensor and System of Systems Approach *," in *2019 41st Annual International Conference of the IEEE Engineering in Medicine and Biology Society (EMBC)*, 2019, pp. 6132–6135.
[24] S. X. Liu, "Symmetry and asymmetry analysis and its implications to computer-aided diagnosis: A review of the literature," *J. Biomed. Inform.*, vol. 42, no. 6, pp. 1056–1064, 2009.
[25] T.-N. Nguyen, S. Dakpé, M.-C. Ho Ba Tho, and T.-T. Dao, "Real-time computer vision system for tracking simultaneously subject-specific rigid head and non-rigid facial mimic movements using a contactless sensor and system of systems approach," *Comput. Methods Programs Biomed.*, vol. 191, p. 105410, Jul. 2020.
[26] K. Clark *et al.*, "The Cancer Imaging Archive (TCIA): maintaining and operating a public information repository.," *J. Digit. Imaging*, vol. 26, no. 6, pp. 1045–57, 2013.
[27] T.-N. Nguyen, V.-D. Tran, H.-Q. Nguyen, and T.-T. Dao, "A statistical shape modeling approach for predicting subject-specific human skull from head surface," *Med. Biol. Eng. Comput.*, vol.58, In Press, Jul. 2020.
[28] S. Marden and J. Guivant, "Improving the performance of ICP for real-time applications using an approximate nearest neighbour search," *Australas. Conf. Robot. Autom. ACRA*, pp. 3–5, 2012.
[29] A. Myronenko and X. Song, "Point set registration: Coherent point drifts," *IEEE Trans. Pattern Anal. Mach. Intell.*, vol. 32, no. 12, pp. 2262–2275, 2010.
[30] A. S. Householder, "Unitary Triangularization of a Nonsymmetric Matrix," *J. ACM*, vol. 5, no. 4, pp. 339–342, Oct. 1958.
[31] N. Aspert, D. Santa-Cruz, and T. Ebrahimi, "MESH: measuring errors between surfaces using the Hausdorff distance," in *Proceedings. IEEE International Conference on Multimedia and Expo*, 1978, pp. 705–708.
[32] A. Fabri, G.-J. Giezeman, L. Kettner, S. Schirra, and S. Schnherr, "On the design of CGAL a computational geometry algorithms library," *Softw. Pract. Exp.*, vol. 30, no. 11, pp. 1167–1202, Sep. 2000.
[33] H. Li, Z. Xie, S. Ruan, and H. Wang, "The measurement and analyses of symmetry characteristic of human skull based on CT images," *Sheng wu yi xue Gong Cheng xue za zhi= J. Biomed. Eng. Shengwu Yixue Gongchengxue Zazhi*, vol. 26, no. 1, pp. 34–37, 2009.

Vi-Do TRAN received the Ph.D in BioRobotics, Scuola Superiore Sant'Anna di Pisa, Italy, in 2019. His research interests are in the fields of rehabilitation robotics, assistive technologies, human-robot interaction and biomechanical simulation.

Tien Tuan Dao is Full Professor in Biomedical Engineering and Biomechanics at Centrale Lille Institut, France since 2020. His research interests concern computational biomechanics, knowledge and system engineering, and in silico medicine.

Tan-Nhu NGUYEN received the Ph.D in Biomedical Engineering and Biomechanics at Université de technologie de Compiègne, France, in 2020. His current research interest is muscle modeling coupled with serious game for facial rehabilitation.